A Lightweight Joint RIS/BS Configuration Scheme

Antoine Dejonghe, Zwi Altman, Francesco de Pellegrini, Eitan Altman

A Lightweight Joint RIS/BS Configuration Scheme

Antoine Dejonghe[†⋆], Zwi Altman[†], Francesco De Pellegrini[⋆] and Eitan Altman[⋆*]

***Abstract*—The integration of RIS elements in upcoming 6G networks appears a major breakthrough to extend network coverage and capacity. This paper introduces a new link-layer scheme for RIS-enabled communications building on existing models for the physical layer of RIS technologies. The scheme is able to integrate the selection of precoders/beams in a codebook and scheduling of UEs at once. Furthermore, elements for the integration of the proposed scheme in current 3GPP-5G specifications are addressed. The scheduler combines a slow mechanism operating at the downlink OFDMA frame scale with a standard proportional fair scheduler operating at the OFDMA slot scale and accommodating both LOS and non-LOS UEs. We introduce an optimization framework for the proposed scheduler whose performance is hence simulated in a reference scenario. The spectral efficiency figures in our tests confirm a large gain of the scheme against a baseline direct path scheme. Finally, the scheduler optimization permits to achieve a further improvement of 15-20% for non line-of-sight users.**

***Index Terms*—Reconfigurable Intelligent Surfaces, proportional fair scheduler, convex optimization.**

I. Introduction

Researchers in wireless communications are currently developing the future sixth mobile Generation (6G) [1]. It should permit new applications (e.g. haptic communications) which might result in an exponential growth of the energy consumption. To tackle this issue, a new technology called Reconfigurable Intelligent Surface (RIS) has recently received a lot of attention. RISs are devices composed of numerous electronically controllable Reflecting Elements (REs) [2].The reflection coefficient of each RE of a RIS can be tuned electronically to modify the propagation of impinging radio-waves: for instance, a RIS can be used to reflect them in specific directions.

The deployment of RISs is expected to enable a wide range of applications such as cell coverage enhancement, interference mitigation and/or channel rank improvement. The aim is to increase mobile networks' performance – e.g., capacity or energy efficiency – by substantially improving User Equipments' (UEs) Signal to Noise Ratio (SNR).

[†]Orange Labs, Chatillon, France, ⋆University of Avignon, France, [*]INRIA, Sophia Antipolis, France

Recently, several authors have studied RISs from a Physical (PHY) layer point of view. The standard system in this context is a multi-antenna Base Station (BS) coupled to a RIS, as depicted in Fig. 1. The BS and the RIS precoders are jointly designed in order to maximize UEs' SNR [3]- [7], [12]. Some variants of the baseline configuration have been studied as well, encompassing different numbers of UEs and RISs, and single or multiple antennas at the BS and UEs.

The joint design of optimal BS and RIS precoders usually requires to solve a non-convex optimization problem [3]. It is standard practice to cope with the complexity of the related algorithmic-based solutions using Machine Learning (ML) tools, such as Deep Learning [6]. We observe that only a few works in the literature address link-layer aspects (e.g., power control [5]) typically deriving theoretical performance bounds.

In this paper we present a novel efficient and low-complexity solution to configure RISs, namely the *RIS configuration pattern* (RCP). An RCP consists of a predetermined periodic sequence of precoders with fixed duration. The precoders used in the RCP are drawn from a codebook. Each precoder can be allocated a different time duration within the RCP period. Based on the proposed RCP working principle, we present two schemes. In the first scheme, the RCP corresponds to a nominal time allocation pattern which is assigned apriori. In the second scheme, the allocation of time resources to each RCP precoder is derived from an online convex optimization for each RCP period. The resulting RCP structure adapts to the UEs distribution and maximizes the aggregated UEs' performance.

The RCP structure optimization and UEs' scheduling can be viewed as two embedded control loops. The RCP structure optimization is a *slow* control loop where the RCP structure is only updated every few tens of milliseconds. Conversely, UEs' scheduling corresponds to a *fast* control loop where the RCP structure can be considered fixed in time. In this paper, our main contributions are: (i) the proposed low-complexity RIS configuration scheme, namely, the RCP, (ii) an online convex optimization solution for the RCP structure optimization (i.e. the slow control loop), (iii) an adaptation of a Proportional-Fair

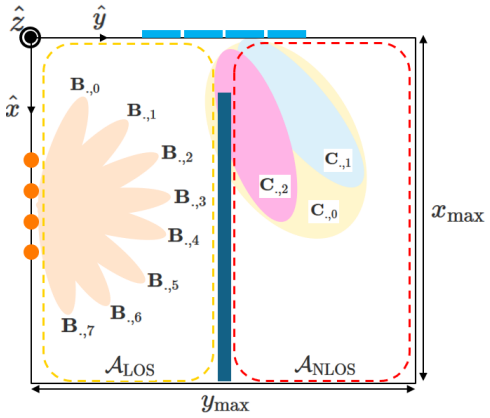

Fig. 1. The baseline system model, orange dots and blue rectangles depict BS antennas and RIS REs, respectively; $N_{\mathbf{B}} = 8, N_{\mathbf{C}} = 3$.

(PF) scheduler to the RCP scheme (i.e. the fast control loop), and (iv) guidelines for the integration of the RCP solution in current 3GPP-5G specifications.

The rest of the paper is organized as follows. Section II details the system model. Sec. III proposes two RIS-assisted network implementations, one of which is compatible with the 3GPP-5G standard. UEs' scheduling and RCP structure optimization are presented in Sec. IV. Simulation results and conclusions are presented in Sec. V and VI, respectively.

II. System Model

We study an outdoor Downlink (DL) scenario for a Multiple Input Multiple Output-Orthogonal Frequency Division Multiple Access (MIMO-OFDMA) system. We consider the baseline two-dimensional (2D) system of Fig. 1, composed of a BS equipped with M antennas (Uniform Linear Array (ULA)) which serves U single-antenna UEs. The system includes a RIS equipped with N REs (ULA) which can assist the communication between the BS and the UEs. The BS-RIS model describes the azimuthal variations of the radiated fields, while Path-Losses (PLs) are considered in 3D. This approach is often used in the literature and allows to achieve meaningful Quality of Service (QoS) results [7].

We assume the BS and the RIS are located at fixed positions, while UEs are mobile. Fig. 1 shows a central obstruction that splits the playground into two equal zones denoted by $\mathcal{A}_{\text{LOS}}$ and $\mathcal{A}_{\text{NLOS}}$. UEs located in $\mathcal{A}_{\text{LOS}}$ experience a Line-of-Sight (LOS) channel with respect to the BS. Conversely, the UEs located in $\mathcal{A}_{\text{NLOS}}$ experience a Non-LOS (NLOS) channel.

We respectively define the sets of UEs, BS antennas, RIS REs and OFDM subcarriers indexes as $\mathcal{U} = \{0, 1, ..., U-1\}, \mathcal{M} = \{0, 1, ..., M-1\}$, $\mathcal{N} = \{0, 1, ..., N-1\}$ and $\mathcal{K} = \{0, 1, ..., K-1\}$ where K is the number of OFDM subcarriers. We also define the time-scale $\mathcal{T}$ whose granularity corresponds to a slot. Finally, we define the indexes $u \in \mathcal{U}$, $m \in \mathcal{M}$, $n \in \mathcal{N}$, $k \in \mathcal{K}$ and $t \in \mathcal{T}$.

A. Channel Model

Two links between an UE $u \in \mathcal{U}$ and the BS are considered, namely a direct link and a cascaded link. For the direct link, the signals transmitted by the BS are received by the UE without being reflected by the RIS. If the UE is located in $\mathcal{A}_{\text{LOS}}$ (resp. $\mathcal{A}_{\text{NLOS}}$), this link is modelled thanks to a LOS (resp. NLOS) channel denoted by $\mathbf{f}_{u,\text{LOS}}^{t,k} \in \mathbb{C}^{1\times M}$ (resp. $\mathbf{f}_{u,\text{NLOS}}^{t,k} \in \mathbb{C}^{1\times M}$). In the sequel, the channel vector $\mathbf{f}_u^{t,k}$ will be written without the subscripts LOS and NLOS for sake of notation. For the cascaded link, the signals transmitted by the BS are reflected by the RIS before being received by the UE. The cascaded link is modelled thanks to two channels: a Free-Space (FS) BS-RIS channel denoted by $\mathbf{H} \in \mathbb{C}^{N\times M}$ and a LOS RIS-UE channel denoted by $\mathbf{g}_u^{t,k} \in \mathbb{C}^{1\times N}$.

In this work, LOS channels are modelled as Ricean channels where channel coefficients simulating a FS path and multiple reflected paths are summed, scaled by a Ricean factor [13]. NLOS channels are only based on channel coefficients simulating reflected paths. LOS and NLOS channels are time-varying, and remain constant during an interval of time smaller than their coherence time T_c. Finally, given the large bandwidth considered, these channels are also frequency-dependent. Therefore, they are expressed in terms of time t and a specific subcarrier k (e.g. $\mathbf{f}_u^{t,k}$).

The BS-UE, BS-RIS and RIS-UE channels are modelled as $\mathbf{f}_u^{t,k} = \sqrt{\beta_{\mathbf{f},u}}\widetilde{\mathbf{f}}_u^{t,k}$, $\mathbf{H} = \sqrt{\beta_{\mathbf{H}}}\widetilde{\mathbf{H}}$ and $\mathbf{g}_u^{t,k} = \sqrt{\beta_{\mathbf{g},u}}\widetilde{\mathbf{g}}_u^{t,k}$, respectively. Here, $\widetilde{\mathbf{f}}_u^{t,k}$ and $\widetilde{\mathbf{g}}_u^{t,k}$ denote small-scale fading channel components, defined according to the 3GPP channel model [13], and $\widetilde{\mathbf{H}}$ is modelled as in [6]. Also, $\beta_{\mathbf{f},u} = \beta_0(1 + d_{\mathbf{f},u})^{-\alpha_{\mathbf{f}}}$ and $\beta_{\mathbf{g},u} = \beta_0(1 + d_{\mathbf{g},u})^{-\alpha_{\mathbf{g}}}$ denote the PL for BS-UE and RIS-UE channels; β_0 is the PL at one meter, $d_{\mathbf{f},u}$ and $d_{\mathbf{g},u}$ are distances and $\alpha_{\mathbf{f}}$ and $\alpha_{\mathbf{g}}$ are PL exponents. $\beta_{\mathbf{H}} = \frac{(\Delta N)^2}{4\pi {d_{\mathbf{H}}}^2}$ denotes the PL for the BS-RIS channel where $d_{\mathbf{H}}$ is a distance and Δ^2 is the area of one RE [6].

B. Signal model

Denote by U_{sch}^t the number of UEs scheduled simultaneously by the BS at time t. Note that, $U_{sch}^t \leq U_{sch}^{max}$ where U_{sch}^{max} is the maximum number of UEs that can be scheduled on a time slot. Let $\mathbf{s}^{t,k} \in \mathbb{C}^{U_{sch}^t \times 1}$ denote the

signal transmitted by the BS on the subcarrier k at time t, with $\mathbb{E}\{|\mathbf{s}_u^{t,k}|^2\} = \frac{P_{tx}}{KU_{sch}^t}, \forall u \in \mathcal{U}_{sch}^t = \{1, 2, ..., U_{sch}^t\}$. P_{tx} denotes the BS total transmit power. At time t, P_{tx} is equally distributed among the K subcarriers and among the U_{sch}^t beams which are simultaneously steered by the BS (i.e., at most one UE is scheduled per beam). The signal received by the UE $u \in \mathcal{U}_{sch}^t$ is modelled as

$$\mathbf{y}_u^{t,k} = \boldsymbol{\xi}_u^{t,k}(\boldsymbol{\psi}) \left(\mathbf{W}_{.,u}^t \mathbf{s}_u^{t,k} + \sum_{v \in \mathcal{U}_{sch}^t \setminus \{u\}} \mathbf{W}_{.,v}^t \mathbf{s}_v^{t,k} \right) + \mathbf{e}_u^{t,k} \quad (1)$$

where

$$\boldsymbol{\xi}_u^{t,k}(\boldsymbol{\psi}) = \left(\mathbf{f}_u^{t,k} + \mathbf{g}_u^{t,k} \text{diag}(\boldsymbol{\psi}) \mathbf{H} \right). \quad (2)$$

In (2), $\boldsymbol{\psi} = [e^{j\psi_0}, e^{j\psi_1}, ..., e^{j\psi_{N-1}}] \in \mathbb{C}^{N \times 1}$ is the RIS precoder, with $\psi_n \in [0, 2\pi] \ \forall n \in \mathcal{N}$. $\mathbf{e}^{t,k} \sim \mathcal{NC}(0, \sigma_e^2 \mathbf{I}_{U_{sch}^t})$ is an additive white gaussian noise.

The BS precoding matrix is denoted by $\mathbf{W}^t \in \mathbb{C}^{M \times U_{sch}^t}$. We consider here that the BS serves UEs via a GoB of $N_\mathbf{B}$ beams denoted by $\mathbf{B} \in \mathbb{C}^{M \times N_\mathbf{B}}$ [8]. The GoB can be modelled by a DFT codebook [11]: it gathers orthogonal precoders which permit to steer beams in all directions. Such a codebook can be constructed as follows: $\mathbf{B} = [\mathbf{b}_0 \ \mathbf{b}_1 \ ... \ \mathbf{b}_b \ ... \ \mathbf{b}_{N_\mathbf{B}}]$ with $\mathbf{b}_b = \frac{1}{\sqrt{M}} \left[1 \ e^{j\frac{2\pi}{N_\mathbf{B}} b} \ e^{j\frac{2\pi}{N_\mathbf{B}} 2b} \ ... \ e^{j\frac{2\pi}{N_\mathbf{B}}(M-1)b} \right]^T \in \mathbb{C}^{M \times 1}$. Note that in (1), $\mathbf{W}_{.,u}^t = \mathbf{B}_{.,b}, b \in \mathcal{B} = \{0, 1, ..., N_\mathbf{B} - 1\}$. We consider that the GoB is used for both control and data channels. It is noted that in comparison with eigen-based beamforming, the GoB implementation does not require to estimate large channel matrices and benefits from a low processing complexity at the expense of lower performance. In the rest of this paper, we drop the time indexes for the sake of simplicity.

III. RIS-ASSISTED NETWORK IMPLEMENTATION

A. BS working principle

We consider a BS deploying a 3GPP-5G OFDM-Time Division Duplexing (TDD) system. The 5G standard provides high flexibility in the configuration of its frame structure. In the following we present a configuration which enables to address three challenges encountered in the deployment of efficient RIS-assisted networks. It is recalled that the RIS configuration modifies the propagation characteristics which in turn modifies: (i) the UEs' achievable rates via the highest available Modulation and Coding Schemes (MCSs), and (ii) the best BS precoders to serve UEs. It is noted that an under or over-estimated MCS or a misaligned BS precoder can lead to QoS degradation or packet losses. The first two challenges

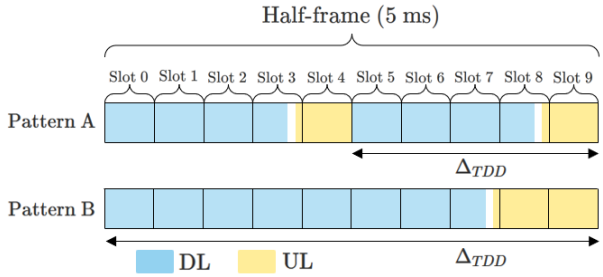

Fig. 2. TDD patterns.

are the ability to rapidly adapt UEs' MCSs and BS serving beams following each RIS reconfiguration. The third challenge is the capability of serving the users with the best available RIS precoders. To address these challenges, frequent performance measurements and Uplink (UL) reports are needed. As explained presently, this is achieved by selecting: (i) a short slot duration (via a high Subcarrier Spacing (SCS)), (ii) a high periodicity of control signals transmissions allowing frequent performance measurements, and (iii) a UL-DL time slot partitioning that supports more frequent UL reports.

BS-UE signalling. In our system, the BS transmits on a carrier bandwidth of W MHz centered around a frequency of f_c GHz. Specifically, it periodically transmits control signals which permit the UEs to measure performance counters. These measurements are reported to the BS for MCS and BS beam determination. We select a SCS of $\mu = 30$ kHz (i.e. a slot lasts 0.5 ms) to shorten the periodicity of control signals' transmissions. This enables frequent UEs' performance measurements.

UE-BS reporting. To enable frequent UEs' performance indicators reporting, we use a specific fixed TDD pattern for UL-DL time slot partitioning [9]. We choose the "Pattern A" (Fig. 2). Compared to other possible patterns (e.g. "Pattern B"), it ensures frequent UL transmissions (i.e. every 2 ms against 4 ms for "Pattern B").

It is noted that frequent UEs' performance measurements and reporting allow to test the performance of numerous RIS configurations in a short timeframe and to select the best one.

B. RIS working principle

We propose presently two-low complexity schemes for RIS configuration. As presented in section II, the RIS REs are configured based on a precoder $\boldsymbol{\psi} \in \mathbb{C}^{N \times 1}$. In this work, the RIS is configured following a predetermined sequence of RIS precoders (Fig. 3), namely the RCP. We assume that an RCP has a fixed duration of F frames and repeats over time. The precoders from the RCP are drawn from a codebook $\mathbf{C} \in \mathbb{C}^{N \times N_\mathbf{C}}$ of

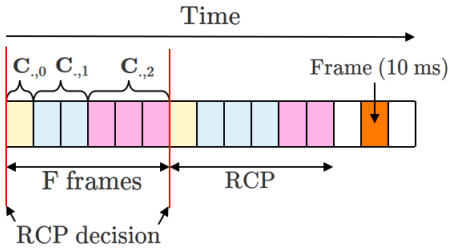

Fig. 3. RIS Configuration Pattern principle, ($F = 6$, $N_{\mathbf{C}} = 3$).

size $N_{\mathbf{C}}$. At any time, we have $\boldsymbol{\psi} = \mathbf{C}_{.,c}$, $c \in \mathcal{C} = \{0, 1, ..., N_{\mathbf{C}} - 1\}$.

We build here a codebook containing few large beams spanning the zone $\mathcal{A}_{\text{NLOS}}$. We assume that the beam directions are configured upon the installation of the RIS. The choice of relatively large RCP beams for covering $\mathcal{A}_{\text{NLOS}}$ ensures that all locations in $\mathcal{A}_{\text{NLOS}}$ are covered frequently enough. Note that the terms precoder and beam are used interchangeably.

Generating large reflected beams with a large RIS composed of many REs is a complex task. To tackle this problem, we adapt here the semidefinite relaxation technique for BS beam synthesis proposed in [14] to the RIS beam synthesis. We encode each precoder weight ($e^{j\psi_n}$) generated based on this technique using z bits [5]. Indeed, current RIS prototypes only admit discrete precoder weights.

Beam coverage. In the proposed scheme we synthesize first one large beam which covers the whole zone $\mathcal{A}_{\text{NLOS}}$. In addition, we design $N_{\mathbf{C}} - 1$ non-overlapping beams, each of which covers a part of $\mathcal{A}_{\text{NLOS}}$ so that the union of the zones covered by these beams corresponds to $\mathcal{A}_{\text{NLOS}}$. Note that by comparing the performance measurements made by an UE when these non-overlapping beams are active, it is possible to determine if the RIS enhances the communications of the UE or not. This information will be exploited by the scheduler as explained later. The large beam and the non-overlapping beams allow both to transmit control signals and data signals to the UEs located in $\mathcal{A}_{\text{NLOS}}$. Fig. 1 depicts a possible codebook $\mathbf{C}$ with $N_{\mathbf{C}} = 3$. The large beam and the $N_{\mathbf{C}} - 1 = 2$ non-overlapping beams are respectively denoted by $\mathbf{C}_{.,0}$ and by $\mathbf{C}_{.,1}$ and $\mathbf{C}_{.,2}$. Let $\mathcal{C}$ denote the set of RIS precoder indexes. We shall use notation $c(t) \in \mathcal{C}$ for the index of the RIS precoder which is active in the RCP at time t.

Network attachment. In the 5G standard, the network attachment procedure corresponds to the transmission of a sequence of control messages between the BS and an UE. According to the system configuration detailed in subsection III-A, this handshake sequence lasts one frame. A successful attachment procedure hence requires the active RIS precoder to remain fixed during an entire frame. Also, for network's performance optimization purpose, it is necessary to frequently make performance measurements on all the precoders which can appear within the RCP. This requires each precoder $c \in \mathbf{C}$ to appear at least once in an RCP.

Precoder Allocation Rules. To ensure the above conditions, we define the following two rules for RCP design. *Rule 1*: each precoder from $\mathbf{C}$ appears only once in an RCP and the order of appearance is fixed. *Rule 2*: the active RCP precoder can only be switched at the beginning of a frame (e.g. switch from $\mathbf{C}_{.,0}$ to $\mathbf{C}_{.,1}$). The above two rules imply that an RCP precoder is active during an integer number of consecutive frames (at least one per RCP).

We investigate two different schemes based on the RCP principle for RIS configuration. The first scheme denoted by "RCP A" corresponds to a fixed RCP structure. The percentage of the F frames composing the RCP allocated to each precoder from $\mathbf{C}$ is constant over time. This scheme has the advantage of being compatible with the 3GPP-5G standard. It is simple and requires no configuration management for the RIS.

The second scheme denoted by "RCP B" uses a flexible allocation of the F RCP frames. To maximize the UEs' performance, the allocation can be adapted to the UEs distribution. For example, more resources can be provided to the RIS beams that serve zones with high UEs densities. In this scheme, the network controller decides at the beginning of each RCP how are the F frames shared among the precoders from $\mathbf{C}$ (i.e., the RCP structure). Each RCP starts with a frame allocated to the precoder $\mathbf{C}_{.,0}$. The network controller exploits the activation time of $\mathbf{C}_{.,0}$ to compute the optimal RCP structure following $\mathbf{C}_{.,0}$ and send it to the RIS. The "RCP B" scheme needs to evolve the management capability to allow: (i) RCP structure computation, and (ii) RCP structure transmission over a management interface. Subsection IV-B details an approach for computing the RCP structure.

C. UEs working principle

We assume that the carrier bandwidth is divided into two non-overlapping parts spreading on K_{data} and $K_{control}$ subcarriers, respectively (i.e. $K = K_{data} + K_{control}$). These parts respectively group most of data and control signals exchanged between the BS and each UE. We denote by $\mathcal{K}_{data}$ and $\mathcal{K}_{control}$ the sets of subcarriers dedicated to data and control signals, respectively.

During all their active period, UEs periodically perform power measurements thanks to the control signals transmitted on the subcarriers from $\mathcal{K}_{control}$. Based on power measurements reported by UEs, the BS can update as frequently as necessary the pairing between UEs and BS beams. We denote by $(u \in b)_c, b \in \mathcal{B}, c \in \mathcal{C}$, an UE $u \in \mathcal{U}$ attached to the BS beam $\mathbf{B}_{.,b}$ when the RIS precoder $\mathbf{C}_{.,c}$ is active. Note that an UE can be attached to different BS beams when different RIS precoders are active. After each power measurement, the beam b to which the UE u is attached, namely $(u \in b)_c$, is determined as follows

$$b = \arg\max_{b' \in \mathcal{B}} \{p_u^{b',c}\}. \tag{3}$$

In (3), $p_u^{b',c}$ corresponds to the power measurement of the UE u when served by the BS beam $\mathbf{B}_{.,b'}$ when the RIS precoder $\mathbf{C}_{.,c}$ is active. $p_u^{b',c}$ is computed as

$$p_u^{b',c} = \frac{P_{tx}}{K_{control} K U_{sch}} \sum_{k \in \mathcal{K}_{control}} \left| \boldsymbol{\xi}_u^k(\mathbf{C}_{.,c}) \mathbf{B}_{.,b'} \right|^2 \tag{4}$$

where $\frac{P_{tx}}{KU_{sch}}$ denotes the power transmitted by the BS on one subcarrier and dedicated to one UE when U_{sch} UEs are scheduled simultaneously. $p_u^{b',c}$ can be interpreted as the mean power received by the UE u on a subcarrier occupied by a control signal. Note that, the expression of the function $\boldsymbol{\xi}_u^k(.)$ is the same than in (2). Therefore, $\boldsymbol{\xi}_u^k(\mathbf{C}_{.,c})$ corresponds to the sum of the direct and cascaded channels on subcarrier k when the RIS precoder $\mathbf{C}_{.,c}$ is active.

Based on (1), we express the Signal to Interference plus Noise Ratio (SINR) of an UE u served by the BS beam $\mathbf{B}_{.,b}$ while the RIS precoder $\mathbf{C}_{.,c}$ is active, on subcarrier k as follows

$$\gamma_u^{b,c,k} = \frac{\frac{P_{tx}}{KU_{sch}} \left| \boldsymbol{\xi}_u^k(\mathbf{C}_{.,c}) \mathbf{B}_{.,b} \right|^2}{\sigma_e^2 + \frac{P_{tx}}{KU_{sch}} \sum\limits_{b' \in \mathcal{B} \setminus \{b\}} \left| \boldsymbol{\xi}_u^k(\mathbf{C}_{.,c}) \mathbf{B}_{.,b'} \right|^2} \tag{5}$$

where σ_e^2 is the noise power.

For sake of simplicity, we assume here that when an UE is scheduled on a given slot, it receives data on all K_{data} subcarriers. Note that multiple UEs can be scheduled on the same time and frequency resources if they can be spatially separated. Therefore, the rate of the UE u served by the BS beam $\mathbf{B}_{.,b}$ when the RIS precoder $\mathbf{C}_{.,c}$ is active can be formulated as follows

$$R_u^{b,c} = \frac{1}{K_{data}} \sum_{k \in \mathcal{K}_{data}} \log_2 \left(1 + \gamma_u^{b,c,k}\right) \quad \text{(bit/s/Hz)}. \tag{6}$$

Note that, the rate achieved on each subcarrier $k \in \mathcal{K}_{data}$ obeys to $\log_2(1 + \gamma_u^{b,c,k}) \leq R^{max}$ where R^{max} corresponds to the Spectral Efficiency (SE) of the highest available MCS.

IV. Problem formulation

The resource allocation for the network with RIS deployment can be viewed as a two control loops optimization problem: (i) a fast loop for UEs' scheduling during which the RCP structure is considered fixed, and (ii) a slow loop that adapts the RCP structure in order to optimize in a fair manner the system sum-rate.

A. UEs' scheduling

We first focus on the fast control loop optimization problem, namely UEs' scheduling with a fixed RCP structure. On each time slot t, the BS serves up to U_{sch}^{max} UEs. At most one UE can be scheduled on each active BS beam on each time slot t (i.e. $U_{sch}^{max} = N_{\mathbf{B}}$). A BS beam is active if at least one UE is attached to this beam. Denote $\mathcal{B}^t$ the set of active beams at time t.

UEs attached to the same BS beam are scheduled based on a PF utility function. This utility function depends on the instantaneous rate of the UE u at time $t+1$ denoted by $R_{u,t+1}^{b,c(t+1)}$ where $(u \in b)_{c(t+1)}$. We define the average rate of the UE u at time t denoted by $\overline{R_{u,t}}$. The average rate at time $t+1$ is computed using exponential moving average with a small parameter ϵ as

$$\overline{R_{u,t+1}} = (1-\epsilon)\overline{R_{u,t}} + \epsilon R_{u,t+1}^{b,c(t+1)}. \tag{7}$$

Note that if the UE u is not scheduled at time $t+1$, the instantaneous rate $R_{u,t+1}^{b,c(t+1)}$ is null. Note also that the average rate $\overline{R_{u,t}}$ is computed over several frames where the UE u can be served by different BS beams and RIS precoders. Finally, the PF scheduling utility function at time $t+1$ denoted by U_{t+1} is expressed as [15]

$$U_{t+1} = V_t + W_{t+1} \tag{8}$$

where V_t and W_{t+1} correspond to the parts of U_{t+1} depending on past scheduling decisions up to time t and on the scheduling decision at time $t+1$, respectively. V_t and W_{t+1} can be formulated as

$$V_t = \sum_{u \in \mathcal{U}} \left[\log(\overline{R_{u,t}} + d) - \epsilon \left(\frac{\overline{R_{u,t}}}{\overline{R_{u,t}} + d} \right) \right] \tag{9}$$

$$W_{t+1} = \left[\epsilon \sum_{b \in \mathcal{B}^t} \max_{(u \in b)_{c'}} \left(\frac{R_{u,t+1}^{b,c'}}{\overline{R_{u,t}} + d} \right) \right]_{c'=c(t+1)} \tag{10}$$

where $d > 0$ is a small constant to avoid problematic behavior near zero.

B. Optimal RCP structure computation

We now focus on the slow control loop optimization problem, namely the computation of the RCP structure. In fact, because the system sum-rate depends on the RIS beams available to UEs, the frequency by which they appear in the pattern must be optimized in a fair manner. To this aim, the adaptive RIS configuration scheme "RCP B" presented in subsection III-B is the core of this slow optimization loop. In the "RCP B" scheme, the network controller decides at the beginning of each RCP how are the F frames of the RCP shared among the $N_{\mathbf{C}}$ RIS precoders from $\mathbf{C}$. We recall that each RIS precoder is activated during at least one frame per RCP (see subsection III-B). This leaves $\tilde{F} = F - N_{\mathbf{C}}$ frames per RCP free to be allocated among available RIS precoders. The RCP structure at time t can be represented by a vector $\boldsymbol{\theta}^t \in \mathbb{R}^{N_{\mathbf{C}} \times 1}$. The entries of $\boldsymbol{\theta}^t$ are the fraction of the $\tilde{F}$ frames allocated to each precoder from $\mathbf{C}$.

$\boldsymbol{\theta}_t$ is determined via an optimization problem that is described presently. Consider an alpha-fair utility function denoted by $X_t^{\alpha}(\boldsymbol{\theta}^t)$. The values of $\boldsymbol{\theta}^t$ that maximize $X_t^{\alpha}(\boldsymbol{\theta}^t)$ permit to achieve a given degree of fairness in terms of rate between time-varying sets of UEs. The design of $X_t^{\alpha}(\boldsymbol{\theta}^t)$ is detailed in the sequel.

The set of UEs $\mathcal{U}$ is partitioned in $N_{\mathbf{C}}$ non-overlapping sets denoted by $\mathcal{U}_c, c \in \mathcal{C}$, such that $\mathcal{U} = \bigcup_{c \in \mathcal{C}} \mathcal{U}_c$ and $\mathcal{U}_c \bigcap \mathcal{U}_{c'} = \varnothing$ for every $c \neq c'$. Set $\mathcal{U}_c$ contains all the UEs whose best RIS precoder is $\mathbf{C}_{.,c}$, i.e., when the corresponding received power under $\mathbf{C}_{.,c}$ is higher than the one under any other precoder from $\mathbf{C}$. The sets $\mathcal{U}_c$ are determined at the end of each RCP based on power measurements as follows

$$\mathcal{U}_c = \left\{ u \in \mathcal{U} \middle| \max_{b \in \mathcal{B}} p_u^{b,c} \geq \max_{b' \in \mathcal{B}, c' \in \mathcal{C} \setminus \{c\}} p_u^{b',c'} \right\}. \quad (11)$$

Define $N_{\mathbf{C}}$ average rates $\overline{R_{u,t}^c}$ for each UE u. These average rates are computed using exponential moving average. However, the sliding window used in order to compute the average rate associated to the UE u and the RIS precoder $\mathbf{C}_{.,c}$ (i.e., $\overline{R_{u,t}^c}$) only comprises the rates of the UE u achieved when the precoder $\mathbf{C}_{.,c}$ was active. In (12), the expression labeled (12.1) corresponds to the sum of the average rates of the UEs from $\mathcal{U}_c$ when served by the RIS precoder $i \in \mathcal{C}$. Note that, for each set $\mathcal{U}_c$, $N_{\mathbf{C}}$ sums are defined as in (12.1). The expression labeled (12.2) in (12) corresponds to a weighted mean of the $N_{\mathbf{C}}$ sums associated to $\mathcal{U}_c$. Specifically, the sum defined in (12.1) for the RIS precoder $i \in \mathcal{C}$ is weighted by the percentage of the F frames which are allocated to the precoder i in the RCP. The role of (12.2) is to provide a measure of the performance of the UEs from $\mathcal{U}_c$ while taking into account the contribution of all the precoders from $\mathbf{C}$. This performance measure is then used to define the utility function $X_t^{\alpha}(\boldsymbol{\theta}^t)$ which can be expressed as in (12) for $\alpha \neq 1$. In (12), $\delta_{|\mathcal{U}_c| \neq 0}$ is the Kronecker index that is equal to 1 if $\mathcal{U}_c$ is not empty and 0 otherwise.

$$X_t^{\alpha}(\boldsymbol{\theta}^t) = \sum_{c \in \mathcal{C}} \frac{\delta_{|\mathcal{U}_c| \neq 0}}{1-\alpha} \underbrace{\left(d + \sum_{i \in \mathcal{C}} \frac{\boldsymbol{\theta}_i^t \tilde{F} + 1}{F} \underbrace{\sum_{u \in \mathcal{U}_c} \overline{R_{u,t}^i}}_{(12.1)} \right)^{1-\alpha}}_{(12.2)} \quad (12)$$

As (12) corresponds to a sum of compositions of concave and affine functions, it can be proven that $X_t^{\alpha}(\boldsymbol{\theta}^t)$ (resp. $-X_t^{\alpha}(\boldsymbol{\theta}^t)$) is concave (resp. convex) in $\boldsymbol{\theta}^t$ for $\alpha \geq 0, \alpha \neq 1$ [16,§A.4.4]. Based on (12), we formulate the convex optimization problem (13a) under affine constraints (13b) and (13c):

$$\min_{\boldsymbol{\theta}^t} \quad -X_t^{\alpha}(\boldsymbol{\theta}^t) \quad (13a)$$

$$\text{subject to} \quad \sum_{c \in \mathcal{C}} \boldsymbol{\theta}_c^t = 1, \quad (13b)$$

$$\boldsymbol{\theta}_c^t \geq 0, c \in \mathcal{C}. \quad (13c)$$

To optimally solve the above problem, we propose here online primal-dual dynamics which aim at minimizing the following Lagrangian

$$L\left(\boldsymbol{\theta}^t, \lambda, \boldsymbol{\nu}\right) = -X_t^{\alpha}(\boldsymbol{\theta}^t) + \lambda \left(\sum_{c \in \mathcal{C}} \boldsymbol{\theta}_c^t - 1 \right) - \boldsymbol{\nu}^T \boldsymbol{\theta}^t \quad (14)$$

where $\lambda \in \mathbb{R}$ and $\boldsymbol{\nu} \in \mathbb{R}_+^{N_{\mathbf{C}} \times 1}$ are the Lagrange multipliers. The update rules for the primal and dual variables write as follows

$$\boldsymbol{\theta}^{s+1} = \left[\boldsymbol{\theta}^s - \eta^s \nabla_{\boldsymbol{\theta}} L(\boldsymbol{\theta}^s, \lambda^s, \boldsymbol{\nu}^s)\right]^{[0,1]} \quad (15a)$$

$$\lambda^{s+1} = \lambda^s + \eta^s \nabla_{\lambda} L(\boldsymbol{\theta}^s, \lambda^s, \boldsymbol{\nu}^s) \quad (15b)$$

$$\boldsymbol{\nu}^{s+1} = \left[\boldsymbol{\nu}^s - \eta^s \nabla_{\boldsymbol{\nu}} L(\boldsymbol{\theta}^s, \lambda^s, \boldsymbol{\nu}^s)\right]^{[0,\infty)} \quad (15c)$$

where $[a]^{[b,c]}$ denotes the projection operator. $\nabla_{\boldsymbol{\theta}} L(\boldsymbol{\theta}^s, \lambda^s, \boldsymbol{\nu}^s)$, $\nabla_{\lambda} L(\boldsymbol{\theta}^s, \lambda^s, \boldsymbol{\nu}^s)$ and $\nabla_{\boldsymbol{\nu}} L(\boldsymbol{\theta}^s, \lambda^s, \boldsymbol{\nu}^s)$ are the gradients of the Lagrangian with respect to $\boldsymbol{\theta}$, λ and $\boldsymbol{\nu}$ at the point $(\boldsymbol{\theta}^s, \lambda^s, \boldsymbol{\nu}^s)$. $\{\eta^s\}_{s \in \mathbb{N}}$ denotes non-summable but square-summable stepsizes. The convergence proof of these primal-dual dynamics will be addressed in a future work.

V. Numerical results

Simulation scenario. Consider a BS and a RIS deployed in a rectangular cell of size $x_{max} \times y_{max}$ where

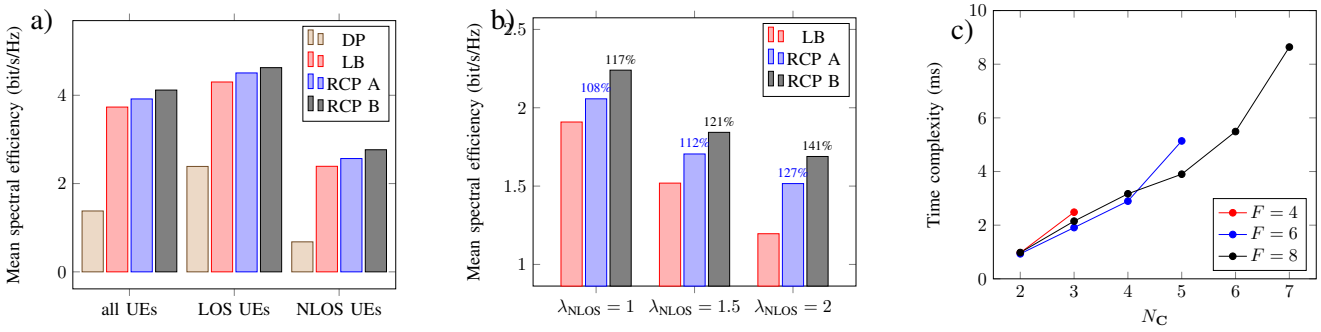

Fig. 4. a) Mean spectral efficiency for the different RIS configuration schemes and UEs' channel conditions, ($\lambda_{\text{LOS}} = 2.5$ UE/s, $\lambda_{\text{NLOS}} = 2$ UE/s); b) NLOS UEs' mean spectral efficiency for the different RIS configuration schemes and NLOS UEs arrival rates, ($\lambda_{\text{LOS}} = 5$ UE/s); c) Time Complexity of the primal-dual dynamics (15a) for different RCP's durations (F) and RIS codebook's sizes ($N_{\mathbf{C}}$).

$x_{max} = 200$ m and $y_{max} = 160$ m, located at $(\frac{x_{max}}{2},0)$ and $(0,\frac{y_{max}}{2})$, respectively. The BS is equipped with $M = 8$ antennas and can steer up to $N_{\mathbf{B}} = 8$ beams simultaneously. The BS transmission power is equal to $P_{tx} = 40$ W. The RIS is equipped with $N = 32$ REs.

The PL coefficients are set to $\alpha_{\mathbf{f}} = 2.7$ (resp. $\alpha_{\mathbf{f}} = 4.1$) for LOS UEs (resp. NLOS UEs) and $\alpha_{\mathbf{g}} = 2.7$. The PL at one meter corresponds to $\beta_0 = -20.4$dB. To model the PL associated to the BS-RIS link, we consider that $\Delta = \frac{\lambda}{2}$ where λ is the wavelength. The small scale fading components $\widetilde{\mathbf{f}}_u^{t,k}$ and $\widetilde{\mathbf{g}}_u^{t,k}$ are generated following the Urban Macro scenario from [13]. The central frequency and bandwidth of the system are set to $f_c = 3.5$ GHz and $W = 20$ MHz, respectively. As the SCS is set to $\mu = 30$ kHz, we have $K = 666$, $K_{data} = 378$ and $K_{control} = 288$.

The traffic process is generated by UEs which enter the playground according to a Poisson process, download a file of size $S = 1$ MB and leave the system when the download is complete. We consider different arrival rates for the $\mathcal{A}_{\text{LOS}}$ and $\mathcal{A}_{\text{NLOS}}$ zones, namely λ_{LOS} and λ_{NLOS} in UE/s. An admission control that accepts up to $U^{max} = 20$ UEs is implemented. The highest MCS used here is the 256-Quadrature Amplitude Modulation so that $R^{max} = 7.4$ bit/s/Hz [10].

Regarding the RCP parameters, we consider a codebook $\mathbf{C}$ with $N_{\mathbf{C}} = 3$ precoders. The RCP lasts $F = 6$ frames and α is set with a value near to 1.

For the sake of comparison, we consider 4 schemes. The first denoted by "Direct Path" (DP) corresponds to the case where no RIS is deployed in the system. The second denoted by "Large Beam" (LB) represents the setting where the RIS continuously steers the large beam from $\mathbf{C}$. The two last schemes correspond to the "RCP A" and "RCP B" introduced in previous sections. In the "RCP A" scheme, the F RCP frames are equally distributed among the $N_{\mathbf{C}}$ precoders.

Performance evaluation. Fig. 4.a) represents the mean SE obtained by all UEs, LOS and NLOS for $\lambda_{\text{LOS}} = 2.5$ UE/s and $\lambda_{\text{NLOS}} = 2$ UE/s. These arrival rates were determined so that the capacity of the system was nearly reached for the worst performing scheme (i.e. "DP" scheme). Interestingly, we infer from Fig. 4.a) that by deploying a RIS, the mean SE is significantly improved for both LOS and NLOS UEs. The RIS reflections directly improve the NLOS UEs' SINRs and hence their mean SEs. This enables the PF scheduler to schedule NLOS UEs less frequently to achieve fairness with LOS UEs, and consequently provide more resources to LOS UEs. This observation is also true when comparing two schemes exploiting RIS reflections, namely the improvement of NLOS UEs' mean SE leads to an improvement of LOS UEs' mean SE.

When setting $\lambda_{\text{LOS}} = 2.5$ UE/s (Fig.4.a)), the schemes "LB", "RCP A" and "RCP B" are far from capacity saturation. Therefore, we also run simulations without considering the "DP" scheme and with higher values for λ_{LOS}. In Fig.4.b), we focus on the mean SE obtained by NLOS UEs for $\lambda_{\text{LOS}} = 5$ UE/s and for different values of NLOS UEs' arrival rate, namely $\lambda_{\text{NLOS}} \in \{1, 1.5, 2\}$ UE/s. The tendency observed in Fig. 4.a) is also observed in Fig. 4.b): we observe though the performance gain with the increase of traffic demand. The mean SE of NLOS UEs when considering the "LB" scheme is enhanced by respectively 27% and 41% with the "RCP A" and "RCP B" schemes.

Complexity analysis. We analyze presently the complexity of the "RCP B" scheme. Two kinds of complexity are considered here, namely the complexity of: (i) the RCP structure computation, and (ii) the RCP structure transmission from the BS to the RIS. Note that, as compared to other RIS configuration schemes from the literature, the "RCP B" scheme only relies on existing 5G low-complexity measurements and do not require

additional channel estimation. Therefore, we neglect the complexity associated to data acquisition.

In order to evaluate the complexity of the RCP structure computation, we measure the average time necessary for the convergence of the dynamics (15a) to the optimal solution of (13a). The impact of the RCP's duration (i.e. F) and the RIS codebook's size (i.e. $N_{\mathbf{C}}$) on time complexity is investigated. To cover all scenarios, we perform Monte-Carlo simulations where the sum-rates labeled as 12.1 in (12) are randomly generated for each Monte-Carlo iteration. Simulations are conducted on a laptop equipped with an AMD Ryzen 5 PRO 3500U w GPU. Results for α set to a value near to 1 are presented in Fig. 4.c). From this figure, we observe that for any value of F and $N_{\mathbf{C}}$, the time complexity remains under the frame duration. This allows the network controller to exploit the activation time of $\mathbf{C}_{.,0}$ (at least one frame) to compute the optimal RCP structure following $\mathbf{C}_{.,0}$ and send it to the RIS (subsec. III-B). From Fig. 4.c), we also infer that for all F values, the time complexity increases with $N_{\mathbf{C}}$. This is due to the increase in the number of operations needed to calculate the gradient at each step of the primal-dual iteration. More precisely, Fig. 4.c) shows that for all F values, the time complexity grows almost linearly for low to medium $\frac{N_C}{F}$ ratios and moderately super-linear for high $\frac{N_C}{F}$ ratios. In the last scenarios, the solutions tend to be located close to the borders of the domain which leads to slower convergence.

Regarding the message complexity of the RCP structure transmission, we observe that for most of the literature's works, the number of bits to be transmitted per RIS reconfiguration equals to $N \times z$ where z is the number of bits used to encode each RIS precoder weight. In our case the number of transmitted bits is much smaller, that is $\lceil \log_2(N_{\mathbf{C}}) \rceil$ for a whole RCP.

VI. Conclusions

In this paper, we presented a new solution for RIS configuration based on a predetermined sequence of precoders drawn from a codebook. Based on this solution, we proposed two low-complexity schemes. The first scheme, compatible with the 3GPP-5G standard, utilizes a fixed sequence of RIS precoders and can be considered as a baseline. The second one is formulated as a convex optimization problem that can be solved online. Its implementation requires to evolve the 5G network management system with a management interface between the BS and the RIS. The numerical results exemplify the added value brought about by the RIS, with performance gain that increases with the traffic demand. It is shown that optimizing the time allocated to the different RIS precoders can significantly enhance performance gain in terms of mean SE. As an example, for relatively high traffic demand, a gain in the order of 40% in SE for NLOS UEs is obtained against a baseline scheme using only a large beam. Future works will focus on learning algorithms rooted in stochastic approximations for the blind online RIS configuration.

References

[1] F. Tariq, M. R. Khandaker, K-K. Wong, et al. A speculative study on 6G. IEEE Wireless Communications, 2020, vol. 27, no 4, p. 118-125.

[2] M. di Renzo, A. Zappone, M. Debbah, et al. "Smart radio environments empowered by reconfigurable intelligent surfaces: How it works, state of research, and road ahead." arXiv preprint arXiv:2004.09352, 2020.

[3] C. Huang, A. Zappone, M. Debbah, et al. "Achievable rate maximization by passive intelligent mirrors." in Proc. of IEEE ICASSP, 2018.

[4] A. Zappone, M. di Renzo, F. Shams, et al. "Overhead-aware design of reconfigurable intelligent surfaces in smart radio environments." arXiv preprint arXiv:2003.02538, 2020.

[5] M. Jung, W. Saad, M. Debbah, et al. "On the optimality of reconfigurable intelligent surfaces (RISs): Passive beamforming, modulation, and resource allocation." arXiv preprint arXiv:1910.00968, 2019.

[6] Ö. Özdoğan et E. Björnson. "Deep learning-based phase reconfiguration for intelligent reflecting surfaces." In : 2020 54th Asilomar Conference on Signals, Systems, and Computers. IEEE, 2020. p. 707-711.

[7] S. Li, B. Duo, X. Yuan, et al. "Reconfigurable intelligent surface assisted UAV communication: Joint trajectory design and passive beamforming." IEEE Wireless Communications Letters, 2020, vol. 9, no 5, p. 716-720.

[8] H. Holma, A. Toskala et T. Nakamura (ed.). 5G technology: 3GPP new radio. John Wiley Sons, 2020.

[9] 3GPP TS 38.213: "NR; Physical layer procedures for control".

[10] 3GPP TS 38.214: "NR; Physical layer procedures for data".

[11] J. Suh, C. Kim, W. Sung, et al. "Construction of a generalized DFT codebook using channel-adaptive parameters." IEEE Communications Letters, 2016, vol. 21, no 1, p. 196-199.

[12] A. Taha, M. Alrabeiah, et A. Alkhateeb. "Enabling large intelligent surfaces with compressive sensing and deep learning." arXiv preprint arXiv:1904.10136, 2019.

[13] "Channel model(s) for 0.5–100 GHz," 3GPP, Sophia Antipolis Cedex, France, TR 38.901., Jun. 2018. [Online]. Available: www.3gpp.org

[14] B. Fuchs. "Application of convex relaxation to array synthesis problems". IEEE Trans. on Anten. and Propagation, 2013, vol. 62, no 2.

[15] R. Combes et al., "Scheduling gain for frequency-selective Rayleigh fading channels with application to self-organizing packet scheduling," Elsevier Performance Evaluation, Vol. 68, Issue 8, Aug 2011.

[16] S. Boyd and L. Vandenberghe. *Convex optimization.* Cambridge university press, 2004.